THE ASTROPHYSICAL JOURNAL, 444:157–164, 1995 May 1

PHYSICAL PROPERTIES OF MOLECULAR CLOUDS IN THE INNER DISK OF M31

R. J. ALLEN,[1] J. LE BOURLOT,[2] J. LEQUEUX,[3,4] G. PINEAU DES FORÊTS,[2] AND E. ROUEFF[2]
Received 1994 July 25; accepted 1994 November 7

ABSTRACT

We discuss recent observations of CO, CS, and NH_3 emission lines from two molecular clouds in the inner regions of M31. The intensities of the $^{12}CO(1–0)$, $^{12}CO(2–1)$, $^{13}CO(1–0)$, and $^{13}CO(2–1)$ lines have been measured with the IRAM 30 m telescope at the same angular resolution of 23″. Upper limits have been obtained in the CS(2–1), CS(3–2) and in the $NH_3(1, 1)$ and (2, 2) lines (the latter two with the Effelsberg 100 m telescope). The line intensities and ratios are compared with the predictions of a one-side UV-illuminated plane-parallel model which treats consistently radiative, chemical, and excitation processes of CO and its isotopes. A satisfactory agreement cannot be achieved for a single-density model. It appears that the emission of the ^{12}CO lines is dominated by a low-density, very cold gas while that of the ^{13}CO lines comes largely from higher density clumps inside the clouds. The properties of the molecular clouds can be understood as resulting mainly from a very small rate of photodissociation due to a very low UV radiation field, together with a low cosmic-ray density. Typical kinematic temperatures inside the clouds can drop to values less than 5 K.

Subject headings: galaxies: individual: (M31) — galaxies: ISM — ISM: clouds — ISM: molecules

1. INTRODUCTION

In a previous paper, Allen & Lequeux (1993) reported observations of emission in the $^{12}CO(1–0)$ and $^{13}CO(2–1)$ transitions from two molecular clouds in the inner disk of the Andromeda Galaxy M31. These clouds are located about 10′ (~2 kpc) from the center of M31. The line widths appear to obey the same relation with cloud size as that of Galactic giant molecular clouds (GMCs), suggesting that one is dealing with the same type of massive (few times $10^7\ M_\odot$) objects. However, the intensity of the $^{12}CO(1–0)$ line is lower by an order of magnitude compared to that of similar Galactic clouds, and the $^{12}CO(2–1)/^{12}CO(1–0)$ line intensity ratio is unusually small. This suggests low temperatures, and thus probably little heating, presumably due to a low intensity of far-UV radiation and a low flux of cosmic rays.

In a paper aimed at understanding the observed temperatures and densities of molecular gas in normal and starburst galaxies, Suchkov, Allen, & Heckman (1993) computed equilibrium kinetic temperatures for molecular clouds heated only by cosmic-ray ionization, and cooled by the molecular line radiation itself. Among other results their calculations showed that, with the low levels of cosmic-ray density expected for the inner disk of, e.g., M31, very low kinetic temperatures can occur over a wide range of density. In fact, for cloud densities less than a few times 10^3 cm^{-3} and an ionization rate of 1/10 or less of that in the Galaxy at the solar radius, the temperatures of the clouds in M31 could drop to near the cosmic background radiation, thereby rendering the clouds virtually invisible in emission. This has led to the suggestion (Allen & Lequeux 1994; Lequeux, Allen, & Guilloteau 1993) that cold molecular gas may make a significant contribution to the dark matter component of disk galaxies.

[1] Space Telescope Science Institute, 3700 San Martin Drive, Baltimore, MD 21218.
[2] DAEC, Observatoire de Paris-Meudon, 92195 Meudon Cedex, France.
[3] DEMIRM, Observatoire de Paris, 61 Av. de l'Observatoire, 75014 Paris, France.
[4] Radioastronomie, Ecole Normale Supérieure, 24 Rue Lhomond, 75231 Paris Cedex 05, France.

The calculations by Suchkov et al. were quite simplified and ignored many important aspects of the radiation transfer, including, e.g., resonant trapping in the CO lines, the dependence of cloud chemistry on ionization, the effects of external UV radiation, etc. In this paper, we present a more detailed model of the physics, chemistry, and radiation transfer in these molecular clouds, and use this model to compute the intensities and ratios of molecular lines for various choices of the basic parameters. In § 2 we briefly present the observations of two molecular clouds in M31 for which we have now measured the four lines $^{12}CO(1–0)$, $^{12}CO(2–1)$, $^{13}CO(1–0)$, and $^{13}CO(2–1)$ at the same angular resolution, as well as sensitive upper limits in the lines of CS(2–1), CS(3–2), $NH_3(1, 1)$, and $NH_3(2, 2)$. Section 3 summarizes the characteristics of the chemical and radiative transfer model we use for predicting the intensities of these lines. Section 4 discusses the properties of the clouds derived from a comparison of the observations with the model predictions, and § 5 contains a discussion and the conclusions of this work.

2. OBSERVATIONS OF CO, CS, AND NH_3

CO observations of the two dust clouds D268 and D478 (Hodge 1980) have been made with the IRAM 30 m telescope at Pico Veleta near Granada (Spain). With this telescope the clouds are resolved; the clouds have sizes of 2.′1 × 1.′2 (D268) and 6.′5 × 1.′1 (D478) in Hodge's catalog, whereas the telescope FWHM is 23″ for the (1–0) lines and 13″ for the (2–1) lines. The ^{12}CO profiles do not change much with position over the image of the dust cloud, and these lines are therefore likely to be optically thick. The ^{12}CO line observations have been reported by Allen & Lequeux (1993).

In order to obtain a meaningful ratio, one position was observed on each of the clouds in the $^{12}CO(1–0)$ line, while the $^{12}CO(2–1)$ line was observed simultaneously at the same position and also in a cross at four neighboring positions offset by 13″. The central position is indicated in the caption of Figure 1 for D478. For D268 it corresponds to offsets (−377″, −524″); see Figure 1*a* of Allen & Lequeux (1993). A simple average of the $^{12}CO(2–1)$ spectra from the five positions (with double

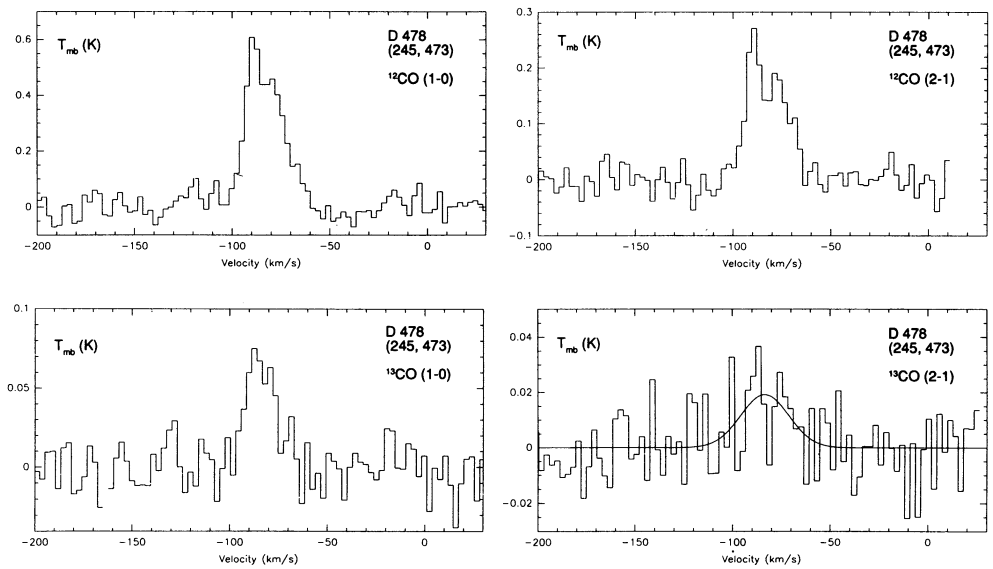

FIG. 1.—CO line profiles for the central position on D478. The position (245,473) is an arcsecond offset in α, δ, from the (1950) adopted center of M31 at $\alpha = 00^h40^m0^s.3$, $\delta = 40°59'43''.0$ (see Fig. 1*b* of Allen & Lequeux 1993). The (2–1) data have been spatially averaged over approximately the same solid angle as the main beam of the (1–0) data. The ^{13}CO(2–1) profile has a low S/N ratio; a least-squares Gaussian fit (with no constraints) is shown for clarity. The parameters of this fit are given in Table 1.

weight for the profile at the central position) closely approximates the telescope beam area covered by the ^{12}CO(1–0) spectrum, hence the observations in the two lines are directly comparable and refer to a 23″ beam. Similar observations have been made in the ^{13}CO(1–0) and ^{13}CO(2–1) lines, with effective integration times of 1.5 and 4.1 hr, respectively (ON + OFF). A preliminary report of these observations and of their interpretation has been presented by Allen & Lequeux (1994).[5] The four spectra obtained for D478 are displayed in Figure 1, in units of main-beam brightness temperature T_{mb}. For D268, we could obtain only an upper limit for the ^{13}CO(2–1) line.

We also made 5.9 hr integrations (ON + OFF) in the CS(2–1) and CS(3–2) lines on D478 and D268 with the 30 m telescope (FWHM ~27″ and ~18″, respectively), but only upper limits could be obtained. Upper limits have also been obtained by T. Wilson in the NH_3(1, 1) and (2, 2) lines with 6 hr integrations (ON + OFF) on both D478 and D268 with the Effelsberg 100 m telescope (FWHM 40″). All these upper limits are reported in Table 3.

Table 1 gives the parameters of the observed lines; the line ratios are in Table 2. The ratios are calculated from the integrated line profiles $I_{CO} = \int T_{mb}\, dV$, rather than from the peak intensities T_{mb} which are less well determined; as the line widths are comparable within the errors (except possibly for the ^{13}CO(1–0) line in D478), this should still provide mutually consistent estimates. As can be seen in Figure 1, D478 exhibits a skewed, perhaps double profile in both ^{12}CO lines, while the ^{13}CO(1–0) line appears to be single and is marginally narrower. The structure of the ^{13}CO(2–1) line is masked by noise at the present level of sensitivity. Our mapping of this cloud suggests that this double ^{12}CO profile arises from variations in the spatial structure (probably the temperature) of the cloud rather than from self-absorption. This complication has been ignored in the following discussion. The line profiles for D268 do not appear split at the present levels of sensitivity and resolution.

[5] There are small differences between the present results and those in Allen & Lequeux (1994) owing to improved reductions of the ^{13}CO(1–0) line on D268, and of the ^{13}CO(2–1) line in both clouds.

TABLE 1

GAUSSIAN PROFILE PARAMETERS

Source Name	CO Line	CO Isotope	Area (K km s^{-1})	Position (km s^{-1})	FWHM (km s^{-1})	Amplitude (Kelvins)
D268.....	1–0	12	3.05 (0.29)	−544.4 (0.5)	11.1 (1.3)	0.26
D268.....	1–0	13	0.28 (0.07)	−542.5 (1.4)	10.2 (3.5)	0.026
D268.....	2–1	12	0.60 (0.12)	−543.8 (0.7)	8.5 (2.4)	0.066
D268.....	2–1	13	<0.24 (3 σ)[a]			
D478.....	1–0	12	12.9 (0.5)	−84.2 (0.4)	22.2 (1.0)	0.55
D478.....	1–0	13	1.32 (0.14)	−84.6 (0.9)	17.4 (2.1)	0.071
D478.....	2–1	12	5.44 (0.19)	−84.1 (0.4)	22.3 (0.8)	0.23
D478.....	2–1	13	0.71 (0.08)	−83.8 (1.6)	27.0 (3.7)	0.025

NOTE.—Gaussian profile parameters for the CO emission from the two dust clouds in M31; profile intensities are shown in the T_{mb} system. Bracketed values are 1 σ errors. The angular resolution is 23″.

[a] Assumes FWHM same as that of the ^{12}CO(1–0) line.

TABLE 2

LINE RATIOS FOR M31 DARK CLOUDS

Source Name	^{12}CO(2–1)/ ^{12}CO(1–0)	^{13}CO(2–1)/ ^{13}CO(1–0)	^{12}CO(1–0)/ ^{13}CO(1–0)	^{12}CO(2–1)/ ^{13}CO(2–1)
D268.....	0.20 (0.04)[a]	<0.86	10.7 (3.0)	>2.5
D478.....	0.42 (0.02)[a]	0.54 (0.08)[a]	9.8 (1.1)	7.6 (0.90)

NOTE.—Line ratios for M31 dark clouds, T_{mb} amplitude scale, profile areas used from Table 1. Bracketed values are 1 σ errors, limits are 3 σ.

[a] Statistical error, due to noise only. A further uncertainty of about 20% comes from the relative calibration uncertainties at 2.6 and 1.3 mm; see text § 2.

The accuracies in the ^{12}CO(2–1)/^{12}CO(1–0) line intensity ratios (high S/N observations) are determined by the accuracies in the absolute calibrations at 230 and 115 GHz and are estimated to be of the order of ±20%. The ^{12}CO(1–0)/^{13}CO(1–0) ratios are more dependent on the poorer S/N ratio of the ^{13}CO(1–0) observations and less dependent on absolute calibration, but are nevertheless of the same magnitude. The ^{13}CO(2–1)/^{13}CO(1–0) ratios are affected both by the accuracies in the absolute calibrations and the low S/N ratios and are not known to better than 30%. This must be kept in mind when comparing the observed ratios to the results of model calculations. When comparing the CS and NH_3 observations with the CO data, one should keep in mind that here also the relative calibration uncertainties limit the accuracy to ±20% in the line ratios.

3. THE MODEL

We have constructed self-consistent plane-parallel numerical models of a uniform-density molecular cloud illuminated on one side by isotropic UV radiation. A transition region from atomic to molecular gas appears at the surface, corresponding to the balance between the chemical formation of molecules and their photodestruction. The radiation field is taken to be the "standard" mean interstellar field for the solar neighborhood of Mathis, Mezger, & Panagia (1983) multiplied a factor χ, characterizing the radiative environment of the region studied. Our particular choice of the initial abundances and depletion factors of the various constituents is discussed in § 4. The abundances of the atomic and molecular species are calculated iteratively, as a function of the optical depth inside the cloud, with a steady state model which is an extension of the physico-chemical model for the envelopes of dark clouds described in Le Bourlot et al. (1993). Both UV continuum absorption (due to the grains) and UV line absorption (especially the H_2 Lyman- and Werner-band dissociating lines) are treated as described in Abgrall et al. (1992). The absorption-predissociating lines of CO and of its isotopic substitutions (^{13}CO, C^{18}O) are also included in the model (Le Bourlot et al. 1993).

TABLE 3

UPPER LIMITS ON CS AND NH_3 LINES

Object	CS(2–1)	CS(3–2)	NH_3(1, 1)	NH_3(2, 2)
D268.....	<0.086	<0.087	<0.016	<0.016
D478.....	<0.055	<0.056	<0.010	<0.010

NOTE.—Upper limits (3 σ) on the CS and NH_3 lines for M31 dark clouds in the T_{mb} amplitude scale, assuming the same line width as that of the ^{12}CO(1–0) transition.

3.1. *Thermal Equilibrium and Line Emission*

The temperature of the gas is determined iteratively at each point in the cloud as a function of visual extinction A_V, assuming thermal balance. In the envelope of the cloud, the gas is mainly heated by the photoelectric effect on dust grains and polycyclic aromatic hydrocarbons (PAHs) (Hollenbach, Takahashi, & Tielens 1991; Verstraete et al. 1990), by the formation of H_2 on grain surfaces (Duley & Williams 1986), and by the photoexcitation of H_2 and the photoionization and photodissociation of atoms and molecules (Abgrall et al. 1992). Deeper inside, in the darkest parts of the cloud, the heating of the gas is due only to cosmic-ray ionization and to the energy released by exothermic chemical reactions. We also take into account the heat exchange between the gas and dust grains; however, the temperature of the dust itself is not calculated in a self-consistent way here. This has little influence on the results, as will be discussed in § 4.

The dominant cooling processes included in the model are radiative cooling through collisional extinction of the fine-structure transitions of Si II, C II, C I, and O I, and through extinction of rotational transitions of OH, H_2O, and CO and its isotopic substitutions for which the 15 lowest rotational levels are considered. The ro-vibrational transitions of H_2 are also included in the calculations taking explicitly into account the first 150 ro-vibrational levels with $J \leq 15$, keeping the cascade formalism only for the remaining upper levels of the ground state. A more extended description of all these processes is given in Le Bourlot et al. (1993). The treatment of radiative transfer in the fine-structure and molecular rotational lines is included with escape probabilities of the photons calculated in the "on-the-spot" approximation of de Jong, Dalgarno, & Boland (1980). This is similar to a large-velocity gradient (LVG) calculation, and our results showed good agreement with those of a LVG program. We assume that the external radiation field at millimeter wavelengths is that of the cosmic blackbody at 2.73 K. The resulting line intensities are given as average Rayleigh-Jeans temperatures in the half-space external to the cloud surface; the observed quantity which most closely approximates these intensities is T_{mb}.

3.2. *The Chemical Network*

A total of 74 species was included in the chemical network, including the ^{13}C and ^{18}O isotopic substitutions of CO. Unfortunately, the chemistry of sulfur and nitrogen is not included; this has a negligible effect on the thermal balance, but prevents us from computing the abundances (and therefore the line strengths) of NH_3 and CS. The chemical library comprises 774 reactions including photoprocesses and isotopic substitutions (see the Appendix and Table 1 in Le Bourlot et al. 1993).

4. COMPARISON OF OBSERVATIONS WITH THE MODEL

As with any existing model, our idealized constant-density slab is not a realistic representation of an *actual* cloud, which will most likely have a complicated structure. The main virtue of the slab model is that it allows the explicit introduction of the detailed photophysical processes and provides some understanding of the basic physics. To start the calculation, we have to assume values for the different parameters that characterize molecular clouds in the inner regions of M31. The choice of these parameters rests on the following considerations.

1. The heavy-element abundances relative to n_H, with $n_H = n(H\ I) + 2n(H_2)$, and the grain-to-gas ratio are probably larger

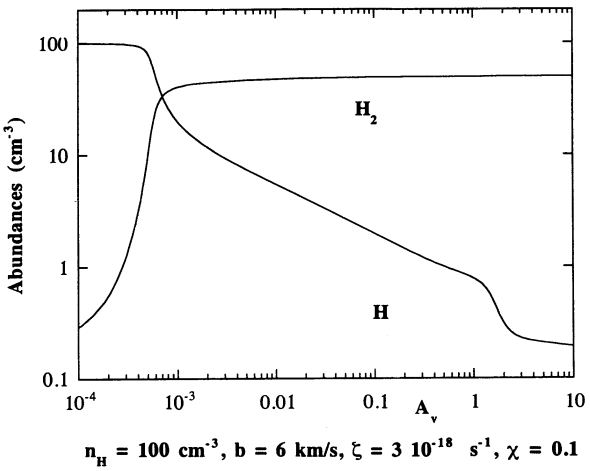

FIG. 2.—Abundances of H_2 and H I in a plane-parallel, uniform, static low-density M31 slab "cloud" model illuminated from one side by a UV radiation field 0.1 times the standard Galactic value. The abscissa is the visual extinction A_V in mag. Owing to the low level of the radiation field, the transition H I–H_2 occurs at very low optical depths. Note the residual H I deep inside the cloud, due to the direct and indirect effects of low-energy cosmic rays (ionization rate $\zeta = 3 \times 10^{-18}$ atom^{-1} s^{-1}).

in the inner regions of M31 than in the Galactic ISM, although they are poorly determined (Blair, Kirshner, & Chevalier 1982). We adopted the following abundances in the gas phase (thus accounting for depletion): $[C]/[H] = 3.62 \times 10^{-4}$; $[O]/[H] = 8.53 \times 10^{-4}$. For the cooling we also use $[Si]/[H] = 3.6 \times 10^{-7}$, $[Fe]/[H] = 6.45 \times 10^{-6}$, although at the low temperatures of interest here these values are of little importance. Finally we use somewhat arbitrarily the Galactic values for the isotopic abundance ratios $[^{16}O]/[^{18}O] = 500$, $[^{12}C]/[^{13}C] = 90$; this may underestimate the amount of ^{13}CO by an unknown amount, perhaps up to a factor 2. The dust-to-gas ratio is assumed to be $N_H = N(H\ I) + 2N(H_2) = 1 \times 10^{21} \times A_V$ cm^{-2} mag^{-1}, where N_H is the total column density of hydrogen and A_V is the visual extinction.

2. The far-UV flux is certainly very weak in these regions which contain few hot stars except at the very center of M31; this can clearly be seen in the UV images published by Hill et al. (1993). We choose, somewhat arbitrarily, a far-UV flux 1/10 ($\chi = 0.1$) that of the standard local Galactic value given by Mathis et al. (1983); the effects of changes in this quantity are discussed later.

3. The flux of low-energy cosmic rays is also likely to be reduced, similar to the UV flux, as those particles are believed to be accelerated in remnants of supernova whose progenitors are massive stars (at least for Type II and Ib supernovae). The cosmic-ray flux is characterized by the ionization rate ζ; the local Galactic value is probably a few times 10^{-17} atom^{-1} s^{-1} and we assume for a start $\zeta = 3 \times 10^{-18}$ atom^{-1} s^{-1}. Low values are justified by the low radio continuum surface brightness observed in the inner regions of M31 compared to the face-on surface brightness of the Galactic disk in the solar neighborhood. The effects of changes in ζ are discussed later.

4. Although the far-UV flux is low, the dust is nevertheless thought to be warm because of heating by the visible radiation from bulge stars (Walterbos & Schwering 1987). We assume a dust temperature of 30 K; the exact value is of minor importance and the results would be essentially unchanged if, for example, the dust temperature was smaller by a factor 2. The visible-UV extinction law is assumed to be Galactic (Fitzpatrick & Massa 1988).

5. The Doppler parameter $b = 2^{1/2}\ \sigma$, with σ the rms velocity dispersion, has initially been taken as a compromise between the observed line widths of D478 and D268; the FWHM for a Gaussian line shape is $1.665 \times b$. The results are not very sensitive to the exact value, provided it is of this order. Later, we compute a model with $b = 3$ km s^{-1}.

Figures 2 and 3 show the results for a low-density model with $n_H = 100$ atoms cm^{-3}. Figure 2 illustrates the H I–H_2 transition zone, which occurs very near the surface of the cloud since the far-UV flux is so weak. Note that there is nevertheless some atomic hydrogen left in the inner parts of the cloud due to direct and indirect dissociation by cosmic rays (de Jong 1972; Sternberg, Dalgarno, & Lepp 1987). Figure 3*a* also illus-

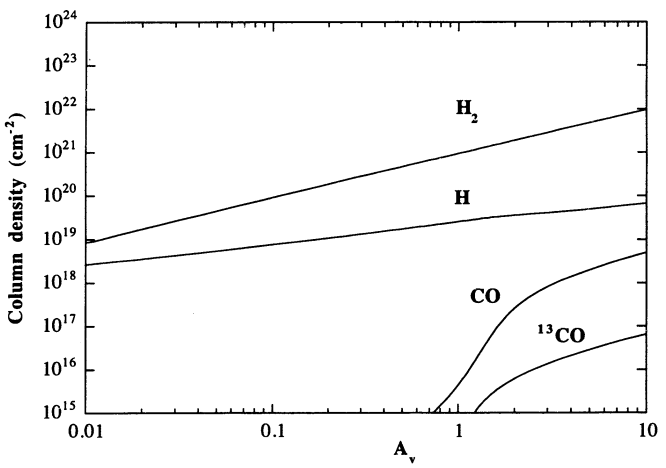

FIG. 3*a*

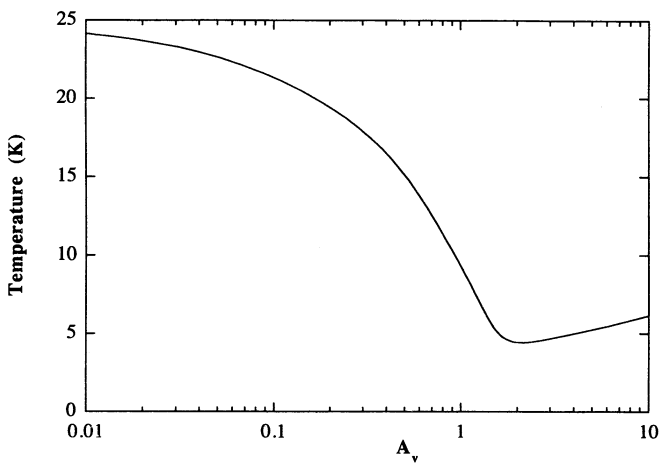

FIG. 3*b*

FIG. 3.—Column densities of several constituents (Fig. 3*a*) and kinetic temperature of the gas (Fig. 3*b*) as a function of distance (expressed as A_V in mag) into the cloud from the UV-illuminated surface. Note the drop in temperature from $A_V = 1$–2 owing to cooling by CO line emission, and the slight rise of temperature deeper inside the cloud owing to increased resonant trapping, with cosmic-ray heating balanced by cooling in the isotopomers of CO.

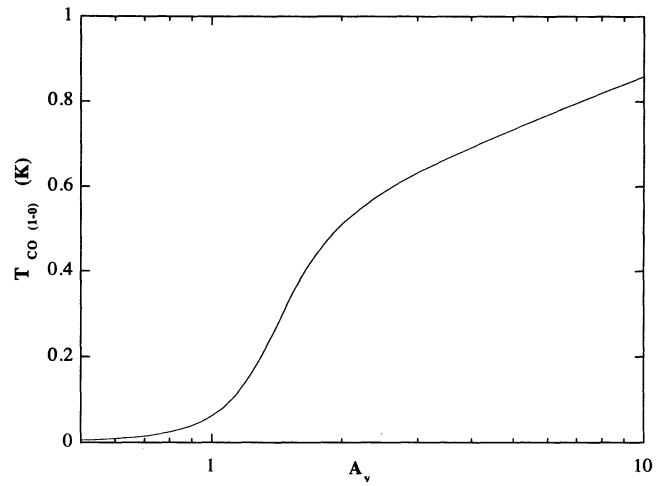

FIG. 4a

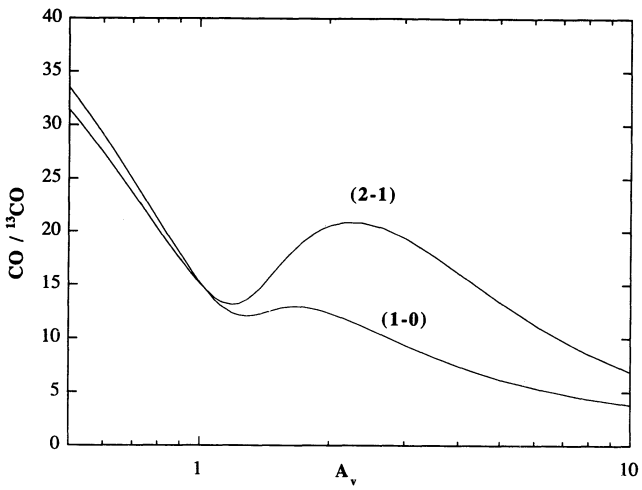

FIG. 4b

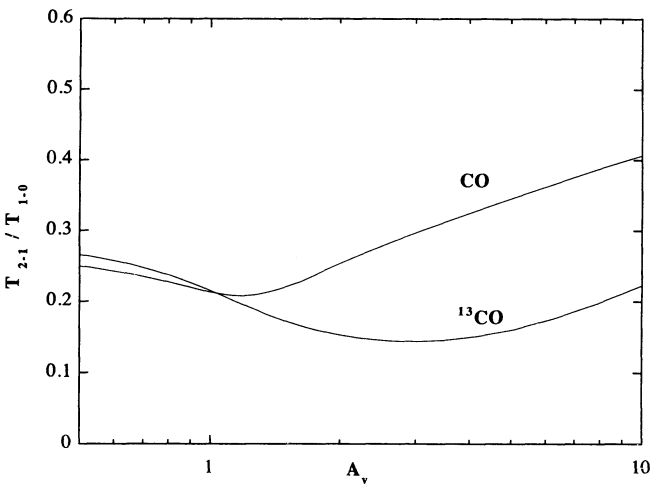

FIG. 4c

FIG. 4.—Computed brightness T_{mb} and ratios of line areas in the $^{12}CO(1–0)$, $^{12}CO(2–1)$, $^{13}CO(1–0)$, and $^{13}CO(2–1)$ lines as seen from an external observer, as a function of A_V. (*a*) Rayleigh-Jeans brightness temperature in the $^{12}CO(1–0)$ line. (*b*) $^{12}CO(1–0)/^{13}CO(1–0)$ and $^{12}CO(2–1)/^{13}CO(2–1)$ line intensity ratios. (*c*) $^{12}CO(2–1)/^{12}CO(1–0)$ and $^{13}CO(2–1)/^{13}CO(1–0)$ line intensity ratios.

trates the H I–H_2 transition, plotted as integrated column densities of the two species as a function of A_V depth inward from the surface of the cloud. The column densities of ^{12}CO and ^{13}CO are also displayed in this figure: both species appear in measurable quantities at $A_V \approx 2$ mag.[6] Figure 3*b* shows the run of the kinetic temperature as a function of depth. Due to the very low UV flux the temperature inside the cloud is essentially determined by the cosmic-ray heating for $A_V > 2$ mag, and is about 5 K for this choice of model parameters. It rises toward the inside of the cloud due to increasing optical thickness and subsequent resonant trapping of the radiation in the cooling lines (mainly CO).

Figures 4*a*, 4*b*, and 4*c* show the evolution of the Rayleigh-Jeans brightness temperature at the center of the $^{12}CO(1–0)$ line, T_{mb}, and of the intensity ratios of the millimeter lines of ^{12}CO and ^{13}CO as a function of A_V, respectively. The $^{12}CO(1–0)$ integrated line intensity $I_{CO} = \int T_{mb}\, dV$ in units of K km s^{-1} can be obtained to a sufficient approximation by multiplying $T_{mb}(1–0)$ by $\pi^{1/2} \times b$ (for a Gaussian line shape). The plotted intensity ratios are the ratios of line profile areas; these are close to the ratios of peak temperatures as the line widths from a given cloud are essentially the same, as indeed is observed. All quantities refer to the integrated emission from all external layers (as seen by an external observer) up to the value of A_V given on the abscissa. The ^{13}CO intensities are probably somewhat underestimated, owing to our neglect of the back-side illumination of the cloud (although we of course do not know if the UV radiation field around the observed clouds is isotropic!). We are presently developing a more realistic model with spherical clouds.

The low-density model indeed predicts very low ^{12}CO line intensity ratios (Fig. 4*c*), even lower than the observed value of 0.4 for D478 at moderate column densities, but somewhat higher than the value of 0.2 observed for D268. The main reason for these low ratios is that, at such low densities, even the $^{12}CO(1–0)$ line is subthermally excited, and this is even more acute for the $^{12}CO(2–1)$ line. The calculated ratio can be raised either by increasing the density or by increasing the cosmic-ray flux, i.e., heating the gas. Figures 5*a* and 5*b* illustrate the large effect of a change in ζ on the kinetic temperature and on the intensity of the $^{12}CO(1–0)$ line, respectively. These results are relatively insensitive to the UV radiation flux; for example, they are essentially unchanged if χ is raised from 0.1 to 0.3.

However, these models (as all low-density models we have calculated) cannot produce $^{13}CO(2–1)/^{13}CO(1–0)$ line ratios higher than the $^{12}CO(2–1)/^{12}CO(1–0)$ ratio (see Table 2), unless the optical depth through the cloud is unrealistically large.[7] This is due to the fact that even a modest UV radiation

[6] The $^{12}CO(1–0)$ line is already optically thick here, with $\tau > 10$ for an excitation temperature of 3.5 K.

[7] Note that, because of the isotopic abundance ratio, the ^{13}CO lines are formed (i.e., $\tau \geq 1$) at much higher values of A_V than required for the ^{12}CO lines, and the slab gets warmer for $A_V > 10$.

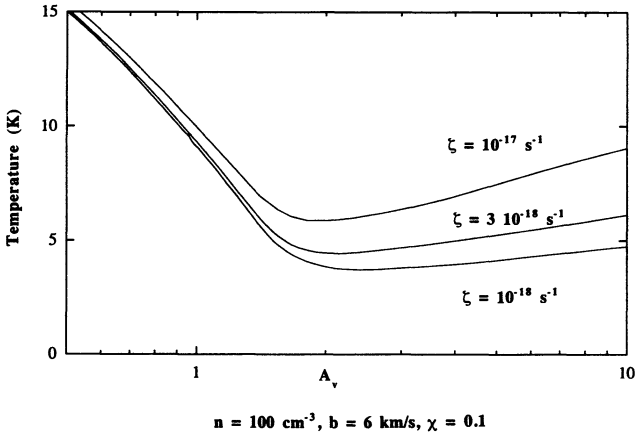

FIG. 5a

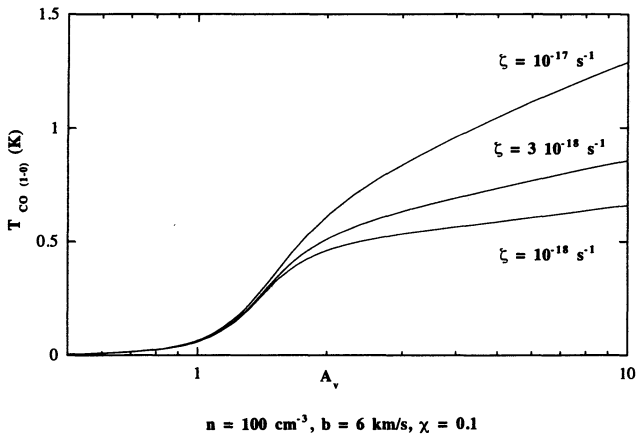

FIG. 5b

FIG. 5.—Effect of the low-energy cosmic-ray flux, as characterized by the ionization rate per atom ζ (label on each curve) on the kinetic temperature (Fig. 5*a*) and on the Rayleigh-Jeans brightness temperature in the ^{12}CO(1–0) line (Fig. 5*b*) as a function of A_V. The model is the same as in Figs. 2–4.

field preferentially heats the outer regions of the clouds where most of the ^{12}CO lines are produced compared to the colder, inner regions where most of the ^{13}CO lines are emitted. A more complicated, two-density model is therefore required. We have calculated higher density models, an example of which is illustrated in Figure 6. This model has a density $n_H = 3 \times 10^3$ cm^{-3}, $\zeta = 1 \times 10^{-18}$, 3×10^{-18}, or 1×10^{-17} atom^{-1} s^{-1}, and a zero UV radiation intensity in order to produce little ^{12}CO emission. This might be appropriate for dense regions deep inside the cloud, which are shielded from external UV radiation by the external layers. We have also used a lower value of the Doppler parameter $b = 3$ km s^{-1}, which is probably more realistic for individual dense clumps inside a molecular cloud. This model predicts rather high ^{13}CO(2–1)/^{13}CO(1–0) ratios for sufficient optical depths (Fig. 6*d*), while the ^{12}CO(1–0)/^{13}CO(1–0) ratios are of the order of 1 (Fig. 6*c*). It is clear that the combination of a low-density model with a high-density one can reproduce the line ratios observed for D478, provided A_V is of the order of 2 mag in the low-density region and 10 mag in the high-density region. For example, a uniform low-density gas with $n_H = 100$ cm^{-3}, $\chi = 0.1$, $\zeta = 3 \times 10^{-18}$, $b = 6$ km s^{-1}, and $A_V = 2$ mag together with a high-density gas having $n_H = 3 \times 10^3$ cm^{-3}, $\chi = 0$, $\zeta = 3 \times 10^{-18}$, $b = 3$ km s^{-1}, $A_V = 10$ mag, and a surface filling factor at a given frequency $f = 0.1$[8] would reproduce rather well the observed line intensities and ratios for D478, but this solution is certainly not unique. The average column densities are about 2×10^{21} H atoms cm^{-2} for the low-density medium, and 1×10^{22} for the high-density medium. The corresponding cloud mass is about $\frac{1}{3}$ of the virial mass determined by Allen & Lequeux (1993); the difference is not significant. Note that, although the surface filling factor of the low-density gas must be nearly unity, it nevertheless cannot fill all of the cloud volume unless the cloud has a flattened, "pancake" shape, as the average thickness of this layer (~ 10 pc) is only about 1/30 the transverse size of the cloud. The column density in the low-density medium of the M31 clouds we study should have a relatively low mean extinction of $A_V = 2 \pm 1$ mag (the small filling factor of the high-density medium is such that it does not contribute much to the mean extinction). Indeed, this is the order of magnitude suggested by Hodge & Kennicutt (1982; see their p. 275) for M31 clouds. Furthermore, Sofue & Yoshida (1993) find a color excess $E(B-V)$ of only 0.2 mag ($A_V = 0.6$ mag) for a smaller dark cloud near the center of M31.[9] Finally, the composite model predicts an abundance of atomic hydrogen of about 1% of that of molecular hydrogen in the diffuse medium, while atomic hydrogen is negligible in the dense medium.

One can, in principle, fix upper limits for the amount of high-density gas in these clouds from our upper limits to the emission in the CS(2–1) and NH_3(1, 1) lines in Table 3 (the upper levels of these species are less useful owing to the low temperatures). For example, the upper limits on NH_3(1, 1) imply 3 σ upper limits of 3 and 2×10^{12} molecules cm^{-2} averaged over the antenna beam for D478 and D268, respectively, assuming that only this level is populated at these low temperatures (Wilson & Mauersberger 1990). If we assume an abundance ratio $N(NH_3)/N(H_2)$ of 2×10^{-8}, appropriate for the Galactic dark cloud TMC 1 with $T_K = 10$ K (Irvine et al. 1987), this in turn implies upper limits of about 1×10^{20} H_2 molecules cm^{-2} or $N_H \approx 2 \times 10^{20}$ cm^{-2} averaged over the antenna beam for a gas with density $n(H_2) > 1 \times 10^4$ cm^{-3}, the critical density for excitation of ammonia. This is marginally compatible with our determination in D478 from the CO lines of $N_H \approx 1 \times 10^{22}$ cm^{-2} at $n_H = 3000$ cm^{-3} [$n(H_2) = 1500$ cm^{-3}]. However, we do not know the abundance of NH_3 at the low temperatures of these clouds; the chemistry is uncertain and NH_3 may be partly frozen on the grains. The constraints for CS refer to gas at even higher densities ($n_H > 1 \times 10^6$ cm^{-3}). For this gas, a reasoning similar to the previous one resting on a comparison with the abundances discussed by Swade (1989a) for the relatively cold Galactic cloud L134N yields a 3 σ upper limit for the column density of H_2 of 1×10^{20} H_2 molecules cm^{-2} averaged over the antenna beam. In dense cores like that of L134N the CS(2–1)/^{13}CO(1–0) line intensity ratio is of the order of 1/20 (Swade 1989b) while it becomes as low as 3×10^{-2} for a more diffuse cloud like Chameleon (Boulanger & Gérin, private communication). On the edges of Galactic molecular clouds, Falgarone et al. (private communication) find a line intensity ratio CS(2–1)/^{12}CO(1–

[8] Note further that the geometrical surface filling factor is $f \times (b_{\rm diffuse}/b_{\rm dense}) = 2f = 0.2$.

[9] We however do not confirm the claim by Sofue & Yoshida for detection of CO in this cloud: see Allen & Lequeux (1993) and Loinard, Allen, & Lequeuex (1995).

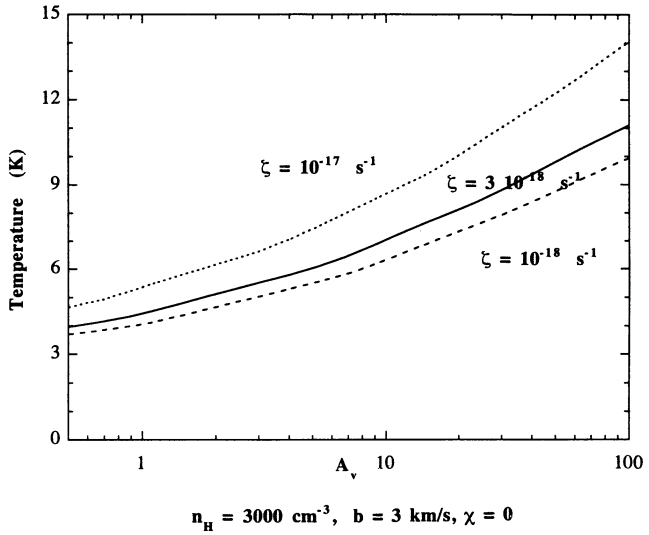

FIG. 6a

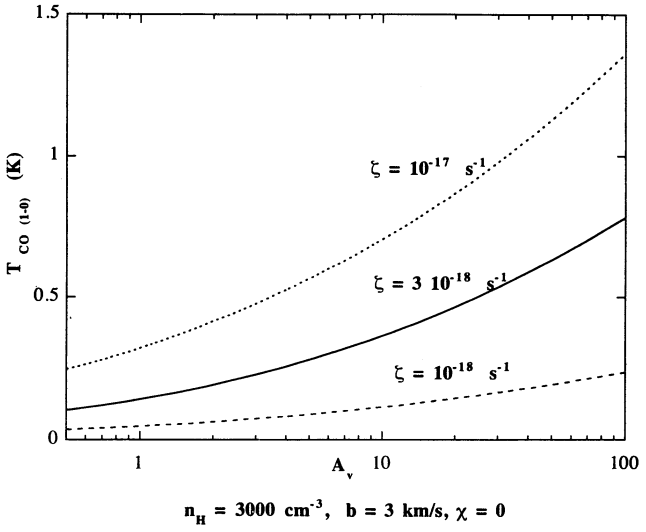

FIG. 6b

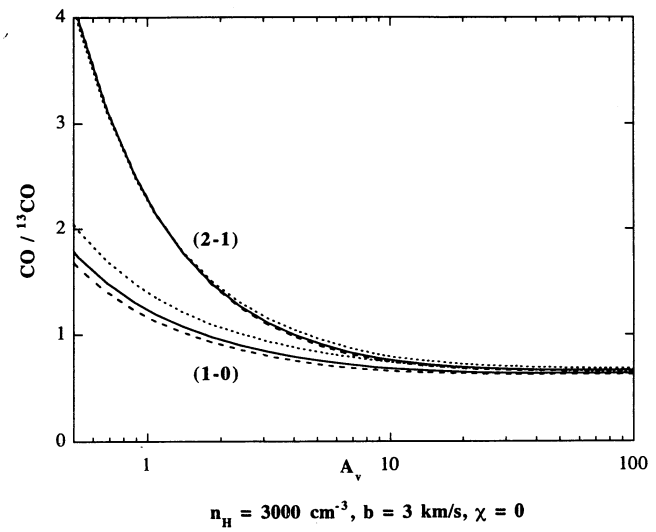

FIG. 6c

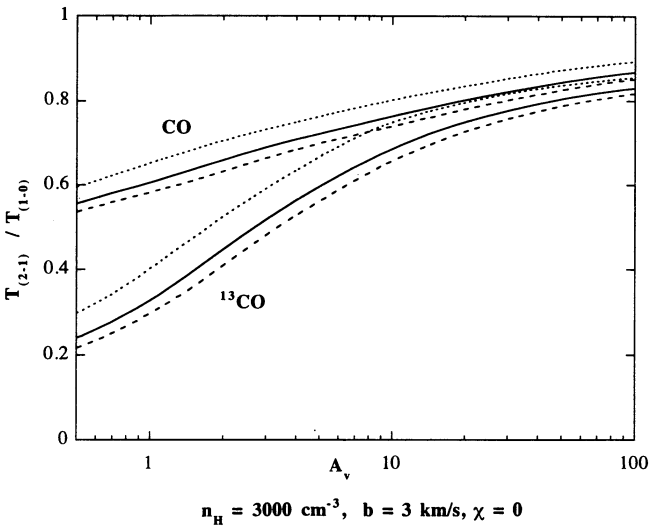

FIG. 6d

FIG. 6.—Results of the model calculations for a plane-parallel, uniform, static, high-density (n_H = 3000 cm^{-3}) slab model. There is no UV radiation; three different values of the cosmic-ray flux are indicated by the values of ζ above each curve. (*a*) kinetic temperature as a function of visual extinction A_V. (*b*) Rayleigh-Jeans brightness temperature in the ^{12}CO(1–0) line. (*c*) ^{12}CO(1–0)/^{13}CO(1–0) and ^{12}CO(2–1)/^{13}CO(2–1) line intensity ratios. (*d*) ^{12}CO(2–1)/^{12}CO(1–0) and ^{13}CO(2–1)/^{13}CO(1–0) line intensity ratios. For Figs. 6*c* and 6*d* the dotted, full, and dashed lines correspond to the same values of ζ as in Figs. 6*a* and 6*b*.

0) = 6 × 10^{-3}. The upper limits we find for these ratios are of the same order and do not give us much new information. In summary, the upper limits we find for the high-density gas are compatible with what we find from CO, but the uncertainties are very large.

Although our observations imply simultaneously a low kinetic temperature and a low density in at least parts of the cloud, they do not supply strong constraints on the physical parameters. Consequently we do not consider it yet worthwhile to try to adjust the models to observations more accurately, especially as the observations of faint lines are rather uncertain. However, a UV flux as large as that in the solar neighborhood can safely be excluded as it would photodissociate CO in the diffuse medium. The cosmic-ray flux is not strongly constrained either, although it is likely to be smaller (and may be significantly smaller) than the value in the Galaxy at the solar radius.

5. DISCUSSION AND CONCLUSIONS: A POSSIBLE "UNIFIED" MODEL FOR MOLECULAR CLOUDS

Our model calculations point to rather extraordinary conditions in the molecular gas associated with dust clouds in the inner regions of M31, conditions which are very different from those found either in our Galaxy or in the Magellanic Clouds. Nowhere else have such low CO(2–1)/CO(1–0) line ratios been seen. We have shown that this implies a low far-UV radiation flux as well as a low flux of low-energy, ionizing cosmic rays, and that the gas is therefore physically very cold. A single-density model cannot reproduce the observed line intensities

and ratios; the ^{12}CO lines come mainly from relatively low density regions ("envelopes"), while the ^{13}CO line emission is dominated by higher density regions ("clumps").

A two-density model is certainly a very rough representation of actual clouds; molecular clouds have a very complex structure, perhaps even hierarchical (Falgarone, Puget, & Pérault 1992), with a large, continuous range of densities. The "very low density region" should be understood merely as representing an average of the low-density parts of the clouds, while the "high-density clumps" represent an average of the higher density regions.

In a given cloud, the density of the rather thin layers where the ^{12}CO lines are formed increases with increasing UV radiation field as the UV photons dissociate the lower density gas; the medium close to this critical density dominates the ^{12}CO line emission since this line quickly becomes optically thick. This is purely an effect of photodissociation in a medium containing a range of densities. For molecular clouds in the Small Magellanic Clouds, where the UV radiation field is at least 10 times that in the solar neighborhood ($\chi > 10$), the density at which most of the ^{12}CO line emission is formed is $0.1\text{–}10 \times 10^4$ cm^{-3} depending on the value of χ (if the UV flux is higher, more of the cloud is dissociated and consequently the remaining molecular regions are denser). The surface filling factor of the dense emitting regions at a given frequency is of the order of 0.1 (Lequeux et al. 1994). In the M31 clouds, on the other hand, the density at which most of the ^{12}CO lines are formed is very low, of the order of 100 cm^{-3}, because the UV radiation field is weak ($\chi \approx 0.1$), and the corresponding surface filling factor is near unity. The situation for our Galaxy is probably intermediate. Thus there is no reason to advocate a different structure for the clouds in the three galaxies on the basis of the ^{12}CO observations alone. However, the optically thinner ^{13}CO lines come from deeper regions and provide additional information. In the SMC, they come from the inner regions of the high-density "clumps" whose surfaces emit the ^{12}CO lines and do not tell us much about the density as the density in these clumps is close to that needed for thermalizing CO. In the M31 clouds, on the other hand, the relatively small ^{12}CO(1–0)/^{13}CO(1–0) intensity ratio and the relatively large ^{13}CO(2–1)/^{13}CO(1–0) ratio imply that the lines of ^{13}CO come from a much denser region than the ^{12}CO line; they are emitted in regions with densities larger than about 3×10^3 cm^{-3}, comparable to the "clumps" in the SMC, although much colder because of smaller UV and cosmic-ray fluxes. Once again, this does not imply a difference in structure. The situation for our Galaxy may be intermediate.

In conclusion, it seems possible that the ISM in different galaxies is basically the same; the changes in the molecular line emission can be accounted for by changes in external parameters (far-UV flux, cosmic rays), and perhaps to a lesser extent in internal parameters (metallicity, dust properties, etc.).

Finally, this paper has confirmed and provided the physical basis for the conjecture that dynamically significant amounts of gas can be effectively "hidden" in massive, cold molecular clouds in galaxies.

We wish to thank T. Wilson for carrying out the ammonia-line observations with the Effelsberg 100 m telescope. R. J. A. thanks the Director of the Space Telescope Science Institute for financial support of the observing trips to Pico Veleta.

REFERENCES

Abgrall, H., Le Bourlot, J., Pineau des Forêts, G., Roueff, E., Flower, D. R., & Heck, L. 1992, A&A, 253, 525
Allen, R. J., & Lequeux, J. 1993, ApJ, 410, L15
———. 1994, in The Nuclei of Normal Galaxies: Lessons from the Galactic Center, ed. R. Genzel & A. Harris (Dordrecht: Kluwer), 105
Blair, W. P., Kirshner, R. P., & Chevalier, R. A. 1982, ApJ, 254, 50
de Jong, T. 1972, A&A, 20, 263
de Jong, T., Dalgarno, A., & Boland, W. 1980, A&A, 91, 68
Duley, W. W., & Williams, D. A. 1986, MNRAS, 223, 177
Falgarone, E., Puget, J. L., & Pérault, M. 1992, A&A, 257, 715
Fitzpatrick, E., & Massa, D. 1988, ApJ, 328, 734
Hill, J. K., Insensee, J. E., Bohlin, R. C., O'Connell, R. W., Roberts, M. S., Smith, A. M., & Stecher, T. P. 1993, ApJ, 414, L9
Hodge, P. W. 1980, Atlas of the Andromeda Galaxy (Seattle: Univ. Washington Press)
Hodge, P. W., & Kennicutt, R. C. 1982, AJ, 87, 264
Hollenbach, D. J., Takahashi, T., & Tielens, A. G. G. M. 1991, ApJ, 377, 192
Irvine, W. M., Goldsmith, P. F., & Hjallmarsson, A. 1987, in Interstellar Processes, ed. D. S. Hollenbach & H. A. Thronson (Dordrecht: Reidel), 561
Le Bourlot, J., Pineau des Forêts, G., Roueff, E., & Flower, D. R. 1993, A&A, 267, 233
Lequeux, J., Allen, R. J., & Guilloteau, S. 1993, A&A, 280, L23
Lequeux, J., Le Bourlot, J., Pineau des Forêts, G., Roueff, E., Boulanger, F., & Rubio, M. 1994, A&A, 292, 371
Loinard, L., Allen, R. J., & Lequeux, J. 1995, A&A, in press
Mathis, J. S., Mezger, P. G., & Panagia, N. 1983, A&A, 128, 212
Sofue, Y., & Yoshida, S. 1993, ApJ, 417, L63
Sternberg, A., Dalgarno, A., & Lepp, S. 1987, ApJ, 320, 676
Suchkov, A., Allen, R. J., & Heckman, T. 1993, ApJ, 413, 542
Swade, D. A. 1989a, ApJ, 354, 828
———. 1989b, ApJS, 71, 219
Verstraete, L., Léger, A., d'Hendecourt, L., Dutuit, O., & Défourneau, D. 1990, A&A, 237, 436
Walterbos, R. A. M., & Schwering, P. B. W. 1987, A&A, 180, 27
Wilson, T. L., & Mauersberger, R. 1990, A&A, 239, 305